Innovative technologies for energy production from low temperature heat sources: critical literature review and thermodynamic analysis.

Electronic supplementary information

Contents

S1 Choice of η as performance index **2**

S2 Detailed discussion of the literature for Sect. 3 **4**
S2.1 Thermogalvanic cells (TEC) 4
S2.2 Electrochemical heat engine (TREC) 5
S2.3 Method based on copper-acetonitrile complexation and disproportionation (CuACN) 8
S2.4 Method based on copper-ammonia complexation (TRAB) 9
S2.5 Thermo-osmosis (TO) 10
S2.6 Thermal separation - salinity gradient power (TS-SGP) 12
S2.6.1 Vacuum distillation - pressure-retarded osmosis (VD-PRO) 12
S2.6.2 Vacuum distillation - reverse electrodialysis (VD-RED) . 13
S2.6.3 Vacuum distillation - battery mixing (VD-BattMix) . . . 15
S2.6.4 Vacuum distillation - redox-flow battery (VD-CRFB) . . 16
S2.6.5 Membrane distillation - pressure-retarded osmosis (MD-PRO) 16
S2.6.6 Membrane distillation - reverse electrodialysis (MD-RED) 17
S2.6.7 Thermolysis - pressure-retarded osmosis (TL-PRO) 17
S2.6.8 Thermolysis - reverse electrodialysis (TL-RED) 17
S2.6.9 Thermolysis - microbial reverse electrodialysis RED (TL-microbial RED) 18
S2.6.10 Thermolysis - Battery mixing (TL-BattMix) 19
S2.6.11 Other thermal separation techniques 19
S2.7 Literature references 20

S3 Detailed discussion of the literature for Sect. 4 (multi-effect combination and heat recuperation) **20**
S3.1 Electrochemical heat engine (TREC) 21

S3.2 Membrane distillation - salinity gradient power (VD-SGP) and thermo-osmosis (TO) 21
S3.2.1 Thermo-osmosis (TO) 22
S3.2.2 Membrane distillation - pressure-retarded osmosis (MD-PRO) 22
S3.2.3 Membrane distillation - reverse electrodialysis (MD-RED) 22
S3.3 Vacuum distillation - salinity gradient power (VD-SGP) 22
S3.3.1 Vacuum distillation - pressure-retarded osmosis (VD-PRO) 23
S3.3.2 Vacuum distillation - reverse electrodialysis (VD-RED) . 23
S3.3.3 Vacuum distillation - redox-flow battery (VD-CRFB) . . 23
S3.4 Identification of literature references 24

S4 Comparison between ρ vs. η with theoretical curves 24
S4.1 Thermo-osmosis (TO) 25
S4.2 Membrane distillation - pressure-retarded osmosis (MD-PRO) . . 26
S4.3 Vacuum distillation - reverse electrodialysis (VD-RED) 26
S4.4 Vacuum distillation - redox-flow battery (VD-CRFB) 28
S4.5 Identification of the literature references 29

S5 Considerations on industrial waste heat 29

S6 Cost of solar heat collection 30

S7 Cost per unit surface area 30

S1 Choice of η as performance index

In this review, we compare the energy efficiency η of the various techniques, rather than $\eta_{2nd-law}$. This choice is justified by the following reasons.

In practical realisations, the relevant performance index is the amount of work (representing the revenue in terms of electrical current cost savings) that can be produced from a given amount of installed heat collectors; this is well characterised by η. If the heat source is at a too low temperature, the efficiency is eventually small and the exploitation of the heat becomes economically unfeasible, notwithstanding a good $2nd$-law efficiency $\eta_{2nd-law}$.

In the context of the present review, we must remark that low-temperature heat is never completely "for free". In the small-scale applications mentioned in Sect. 1, the heat collection plant has an Opex which is almost proportional to the delivered heat power. Following the example given for thermal solar plants, a household solar collector of 20 m^2 installed on the roof delivers a maximum of 19 kW of heat around 100°C, under normal illumination. The relevant performance figure of the heat-to-current conversion is how much electrical power is produced by that plant; with a high value of η, e.g. η=5-10%, the electrical power production is 0.95-1.9 kW, with $\eta_{2nd-law}$=30-60%. Having a device which works with an even higher $\eta_{2nd-law}$ but a lower temperature, such that

the power production is lower, would be of no use, e.g. decreasing the temperature to T_H=35°C, with $\eta_{2nd-law}$=70%, would lead to a power production of only 0.38 kW and η=2%. This confirms that the relevant performance index is the energy efficiency η rather than $\eta_{2nd-law}$, although it must be accompanied by the minimum accepted temperature of the heat source.

As already remarked, an important element of discussion is the size and the economic cost of the heat collectors and heat exchangers. As shown in Fig. 7, all the techniques reviewed here require at least two heat exchanges: one from the heat source to the system, and a second from the system to the heat sink (the environment). Due to the temperature drop across the heat exchangers, the actual heat source temperature available to the process is lower than T_H; we call it $T_{proc,H}$, with $T_{proc,H} < T_H$; analogously, we define the actual heat sink temperature available to the process $T_{proc,L}$, with $T_{proc,L} > T_L$. The surface of heat exchangers is proportional to the heat flux, but it is also inversely proportional of the temperature drop ΔT_{he} across the heat exchanger. Roughly assuming ΔT_{he} as a constant, $T_{proc,H} = T_H - \Delta T_{he}$ and $T_{proc,L} = T_L + \Delta T_{he}$. We call $\Delta T_* = T_{proc,H} - T_{proc,L}$ the actual temperature difference available for the process. The presence of ΔT_{he} represents an irreversible process which degrades the available heat. This effect can be quantified in terms of decrease of the Carnot cycle efficiency:

$$\eta < \frac{\Delta T_*}{T_{proc,H}} \approx \eta_C - 2\frac{\Delta T_{he}}{T_H} < \eta_C, \tag{S1}$$

where the approximation is at first order in $\Delta T_{he}/T_H$ and $(T_H - T_L)/T_H$.

We thus see that, in order to tap a relevant fraction of the ideal Carnot cycle, ΔT_{he} must be much smaller than the available temperature difference $T_H - T_L$, which is less than 75 K in the present context: $\Delta T_{he} \ll$75 K. In industrial plants working at high temperature, the temperature drop ΔT_{he} is often much higher, up to hundreds K. Much smaller ΔT_{he} is needed. For example, having a heat source at T_H=100°C, with ΔT_{he}=30 K, the actual temperature difference available to the process is only ΔT_*=15 K corresponding to a maximum efficiency η <4%. Decreasing ΔT_{he} is possible but expensive, as the surface and the price is roughly inversely proportional to ΔT_{he}. The trade-off between decreasing ΔT_{he} (and thus increasing the efficiency) and decreasing the heat exchanger surface is particularly relevant in the case discussed in this review, because $T_H - T_L$ is quite small compared to usual values of ΔT_{he}. For the same reason, the heat exchangers represent a relevant part of a plant [1]. As an example, the production of 3 kW of power (as in a household application) requires to handle 60 kW of heat when η=5%. Assuming e.g. a heat transfer coefficient U=1 kW/(m^{2}K) (it depends on the involved physical process) and ΔT_{he}=10 K, the needed surface of heat exchangers is 12 m^2; going down to ΔT_{he}=1 K would require 120 m^2, a very large surface.

Since the two heat exchangers are needed by all the techniques analysed here, they represent a fixed cost for any technique. On one hand, the cost is fixed, so it is not necessary to discuss it separately for each technique. On the other hand, it is a cost, that can be seen as a contribution to the Capex of the

plant proportional to the incoming heat power: this discussion emphasises even more the relevance of using the energy efficiency η as one of the performance indices, rather than the $2nd$-law efficiency $\eta_{2nd-law}$.

S2 Detailed discussion of the literature for Sect. 3

S2.1 Thermogalvanic cells (TEC)

The literature on thermogalvanic cells is too wide to be fully accounted for in this review. Rather, we focus on the citations reported in two reviews, Refs. [2] and [3].

Reference [2] highlights the results of two studies, Refs. [4] and [5], reporting the highest power density and relative efficiency, respectively.

In Ref. [4], a highly concentrated ferri/ferrocyanide electrolyte was used. A power density up to 12 W/m^2 was obtained, with temperatures of 21 and 80°C. At the maximum power output, the efficiency relative to the Carnot cycle was 0.4%, corresponding to an energy efficiency η=0.07%.

Reference [5] reports the study of cell with aqueous ferri/ferrocyanide electrolyte and a carbon nanotube aerogel as electrode material. The highest efficiency relative to the Carnot cycle was 3.95%, with a temperature difference of 51.4 K. This value corresponds to an energy efficiency of 0.56%; it must be noticed that this is not an experimentally measured value, but rather a calculated result. The cell reached a power density of 6 W/m^2. The reported efficiency is much higher than usual for this technique; this is due to the unusually low resistance of the electrolyte, while the Seebeck coefficient, the thermal conductivity and the other performances are in line with literature. From Supplementary Table 3 of Ref. [5], we see that the "effective ion conductivity", used for the calculations, is 1210 mS/cm, with an electrolyte concentration of 0.4 M. By comparison, Fig. 3d of Ref. [6], black line, reports a conductivity of 200 mS/cm, at the same concentration. A similar value is obtained from the ionic conductivity reported in literature [7]. The discrepancy between the literature results and the conductivity reported in Ref. [5] is not explained by the Authors. For this reason we decided not to include the results of Ref. [5] in the literature comparison graph, Fig. 8.

Ref. [3] cites in particular two works in which a high power density was attained, Refs. [8] and [9].

Ref. [8] reports a power density p=1.8 W/m^2 and an exergy efficiency $\eta_{2nd-law}$=1.4%. The temperatures are T_H=65°C and T_L=5°C, so the heat sink temperature is below room temperature (this is an unrealistic assumption). The energy efficiency is η=0.24%.

Ref. [9] reports a TEC based on cobalt redox couple in ionic liquid-solvent mixtures. The temperatures are T_H=130°C and T_L=60°C, so the heat source temperature is above the maximum considered in this review (100°C). The power density is p=0.88 W/m^2. The efficiency is not discussed.

S2.2 Electrochemical heat engine (TREC)

We first discuss the works based on battery-like devices.

Ref. [10] reports several experiments. Some of them are performed using T_L=10°C, which is not relevant in practical cases. We rely on the results reported in the Sect. "Long-term cycling" of Ref. [10], which refer to a realistic case, with T_H=50°C and T_L=20°C. The power density p is not reported in terms of power per cell surface, thus we calculated it from the available data. The energy production was 1.26 J/g. The duration of the cycles is not declared, but it can be easily calculated from the current, 17.9 mA/g, and the specific charge of the whole cell, 32.43 mAh/g (Table 1 of supplemental information of Ref. [10]): charging and discharging steps last for 1.8 h each, giving a cycle period of 3.6 h. This gives a power density of 97 μW/g. It must be noticed that a much larger value of 1.2 mW/g is given in Sect. "Discussion" of Ref. [10]; however, it refers to a faster cycling time, a larger current, and a larger temperature difference than the conditions used in Sect. "Long-term cycling" of Ref. [10] for representing a real case.

In order to translate the result into a power density per surface, it is necessary to evaluate the surface of the cell. We normalize with respect to the CuHCF electrode surface, which is an overestimation with respect to the membrane surface. The CuHCF loading is 2.5 mg per 0.25 cm^2 of carbon cloth, i.e. 40 g/m^2. Using the specific charge of CuHCF, 60 mAh/g (Table 1 of supplemental information of Ref. [10]), the specific capacity is 2400 mAh/m^2. Such a capacity corresponds to 74 g/m^2 of total active material, according to the specific charge of the whole cell, 32.43 mAh/g (Table 1 of supplemental information of Ref. [10]). The value of 74 g/m^2 allows us to translate the power density of 97 μW/g into p=7 mW/m^2. Ref. [2] reports a much higher power density for TRECs, probably based on hypothetically larger mass loadings.

According to Table 1 of supplemental information of Ref. [10], the heat capacity of the whole cell is 2.048 J/(K g); the sensible heat needed for heating the cell from T_L=20°C to T_H=50°C is thus Q_{HX}=60 J/g (see Eq. 36 of supplemental information of Ref. [10]). The heat Q_H is instead evaluated according to Eq. 37 of supplemental information of Ref. [10], with α_C=1.19 mV/K, $Q_{c\ ch}$=32.43 mAh/g (Table 1 of supplemental information of Ref. [10]) and T_H=50°C. We obtain Q_H=45 J/g. We thus confirm the energy efficiency of 1.7% at 50% of heat recovery. Extrapolated to ΔT_{he}=5 K (see Eq. S8), we get η=2.2%. These values (the reported ones and the calculated here) are however theoretical limits, since they are not measured on a real cell and only take into account the sensible heat of active materials.

It is worth remarking this text [10]: *"A slight shift of the loop is observed, but there is no significant change in the overall shape.* Since the voltage variation with the temperature is small compared with the average voltage, a very slight shift can lead to a complete loss of energy production [11]. It is thus questionable whether the paper reports a real power production.

In Ref. [12] the studied temperatures are T_L=20°C and T_H=60°C. The efficiency reported in the abstract, 2%, refers to the limit of no overpotential, which

means vanishing power production. The energy efficiency η=1.4% is found in Fig. 4 of Ref. [12], for 10 mV overvoltage and heat recuperation efficiency of 70%, which could roughly represent the heat exchanger temperature difference ΔT_{he}=5 K (see Eq. S8). The efficiency reported in Ref. [12] actually represent an upper limit, obtained assuming that the heat capacity of the cell is only due to the active materials: exchanged heats are not experimentally measured on a real cell. Ref. [12] does not report the obtained surface power density p. However, in page 17015, left column, the power is declared to be 1 mW per g of cell material. This is the value reported in Ref. [10] for quite ideal conditions. Thus it seems that Ref. [12] assumes that the power density of the described device is similar to Ref. [10]. Hence, we decide to report the same power density, p=7 mW/m^2, in the literature comparison graph, Fig. 8.

In Ref. [13] the studied temperatures are T_L=15°C and T_H=50°C, so T_L was below the room temperature. The efficiencies are reported for two values of current, 1C and C/2 (as usual in battery literature, C is the current needed to fully charge the cell in one hour). As in the previous papers, the efficiencies are calculated based on a theoretical evaluation of the needed heat, which only takes into account the active materials of the cell, thus neglecting the passive elements. The values are given Table 1 of Ref. [13]. We consider a heat recuperation of 70%, roughly consistent with ΔT_{he}=5 K. The energy efficiencies η are 2.8% and 3.5% for 1C and C/2, respectively. The power density p is not reported, however it can be calculated. In page 6581, right column, the specific energy production per cycle is reported; it is 0.5 and 0.65 mWh/g for 1C and C/2, respectively. The nominal cycle durations are 2 and 4 hours for 1C and C/2, respectively. From these two values, the average specific powers are 0.25 and 0.16 mW/g.

The reported power is normalised by the active material mass; we must translate this into a surface; we decide to normalise by the surface of the NiHCF electrode. This is an overestimation of the power density with respect to the normalisation by membrane surface; this notwithstanding, the resulting power density is very small. In supplemental information of Ref. [13], first page, last line, it is stated that the mass loading of NiHCF is 3 mg/cm^2. Assuming a capacity of 60 mAh/g for CuHCF, from the mass loading we calculate a capacity of 1800 mAh/m^2. In page 6581, left column, last lines of Ref. [13], it is stated that the capacity is 35.4 mAh/g, where the normalisation is with respect to the total active material mass. Using this value, we get the active material mass of 50 g/m^2. This value translates the above-reported power densities of 0.25 and 0.16 mW/g into values of p of 12 and 8 mW/m^2 for 1C and C/2, respectively.

In Ref. [14], only charging and discharging steps were studied and a perfect heat recuperation was assumed. Under this ideal condition, a high 2*nd*-law efficiency $\eta_{2nd-law}$ was calculated, between 50% and 75%. The reported power density was p=6.4 W/m^2. The result is only speculative, since it relies on the assumption of ideal heat exchangers, thus we do not report these performance indices in the literature comparison graph, Fig. 8.

Ref. [15] discusses an alternative scheme, in which the charging step takes place spontaneously (does not consume external work) and is obtained by means of an electrochemical short-circuit carried on by a redox couple. The efficiency

is theoretically calculated (note 10 of supplementary information of Ref. [15]). The power density under real operation is of the order of 1000 W/m^3 (Fig. 13 of supplementary information of Ref. [15]). Although the paper reports the volumetric power density, it does not give enough information to evaluate the power per unit surface of electrode, thus we do not report the data in the literature comparison graph, Fig. 8.

In Ref. [16], a redox-flow battery scheme is used. Rather than performing the thermal cycle on the whole cell, only the electrolyte is thermally cycled. A device with two electrochemical cells connected by a counter-current heat exchanger have been shown. The efficiency versus power curve is reported in Fig. S8 of supporting information of Ref. [16]. It is however a "simulation", according to the caption, and not an experimental measurement. The simulation is done for various values of heat exchanger power, which correspond to a ΔT_{he} much smaller than 5 K, as required here; it is not possible to extrapolate the result to ΔT_{he}=5 K. For these reasons, we do not report the data in the literature comparison graph, Fig. 8.

The efficiencies reported in the papers cited above are only calculated values; the needed heat is calculated only based on the sensible heat of active materials, neglecting the passive components needed to build a real cell. The actual heat capacity of the experimental cell was much higher. The calculations are reliable, but they refer to idealised systems, i.e. they do not take into account the cycling of a real cell but only of some of the components. Moreover, in some of the papers, the charge leakage during a real charge/discharge cycle is not taken into account. For these reasons, the performance indices are reported as "theoretical" in the literature comparison graph, Fig. 8.

The power densities are very small. It must be emphasised that the power densities reported above are based on the cell that was experimentally realised; since the mass loading was typically small, the resulting power density per unit of surface was also small. Although, in principle, much larger mass loading can be used, it is questionable how the increase of mass loading can affect the performances. In particular, it is known that the increase of mass loading is detrimental for the overvoltage. This particular application is particularly sensitive to this problem, since the voltage rise (variation of voltage induced by the temperature) is very small, thus the overvoltage must be kept much smaller than usual, e.g. in batteries.

We discuss now the works based on supercapacitor-like devices.

Reference [17] discusses the energy production from concentration variations (here defined as CDLE) and from temperature variation (here defined as DLPE). The focus of this work is to study the improvement of power production of CDLE adding a thermal cycling, i.e. DLPE, thus most of the result refer to the simultaneous application of CDLE and DLPE. However, some results are given also for the DLPE alone.

From Fig. 8 of Ref. [17], the voltage rise of DLPE alone is of the order of 7 mV, approximately 1/10 of the voltage rise of CDLE+DLPE shown in Fig. 10 of Ref. [17]. Since the cell and load resistances are similar in the two cases, we expect that the power density of DLPE is 1/100 of the power density

of CDLE+DLPE. For the CDLE+DLPE cycle, the reported power density is 40 mW/m^2 (see page 12384, right column, row 5), hence we evaluate a power density p of 0.4 mW/m^2.

Reference [17] does not focus on the optimisation of the performances, thus the efficiency is not reported at all. We evaluated it based on the following reasoning. The power density, expressed as power per mass of electrode material, is 130 mW/kg for CDLE+DLPE (see page 12384, right column, row 5); for DLPE alone, we evaluate 1.3 mW/kg. From Figs. 8-10 of Ref. [17], the cycle time is around 2 minutes. We evaluate that the energy production per cycle is 0.158 J/kg. The thermal cycle is performed between 25°C and 50°C; in order to perform such thermal cycle, the sensible heat of the electrode materials must be provided; we approximate the heat capacitance of the activated carbon with the one of graphite, 0.79 J/g/K; we obtain 19750 J/kg. We thus find that the produced work is 8×10^{-6} times less than the heat needed to perform the thermal cycle, only considering the electrodes. The energy efficiency η is thus much smaller than 8×10^{-6}.

Reference [18] reports an energy density of 2 mJ/m^2, with a cycle period of 1 min (Fig. 2 of Ref. [18]). From this information we evaluate a power density p of 33 μW/m^2. The efficiency was not experimentally evaluated, but the Authors report that, according to their theoretical evaluation, the $2nd$-law efficiency $\eta_{2nd-law}$ should be is 0.002×10^{-3} (page 359, left column, row 7). Since the cycle exploits a temperature variation of 30 K, we evaluate $\eta = 2 \times 10^{-7}$.

In Ref. [19], the efficiency is expressed in terms of a "figure of merit" of the supercapacitor, ξ. It is connected to the energy efficiency through Eq. 3 of Ref. [19]:

$$\eta = \frac{\eta_C}{1 + \eta_C \cdot \xi^{-1}} \tag{S2}$$

where η_C is the efficiency of the Carnot cycle. For the temperature range considered in this paper, 0-60°C, η_C=18%. The experimentally found value of ξ_{exp} is 0.0039. From this value, an energy efficiency of 0.38% is found. However, this value is almost purely theoretical, since no real cycle has been performed. For the same reason, it is not possible to evaluate the power density p.

The efficiency and the power density of the supercapacitor-based techniques are small, or are not even reported in papers; we thus decide not to report them in the literature comparison graph, Fig. 8.

S2.3 Method based on copper-acetonitrile complexation and disproportionation (CuACN)

No evaluation of performances was reported in Ref. [20].

The experimental setup was improved in Ref. [21]. The experimental work concerns only the electrochemical part, while the thermal process is only calculated theoretically. The calculation is however reliable, because the system is quite simple and the calculation is based on well known physical phenomena. The energy efficiency η is 2% and the average power density is 90 W/m^2 (data reported in the abstract).

It must be noticed that this technique requires a heat source at temperature above 160°C, which is above the maximum temperature considered in this review.

S2.4 Method based on copper-ammonia complexation (TRAB)

Ref. [22] reports a peak power density of 126 W/m^2; it is clearly stated that this figure refers to the power per unit "projected electrode area" [23], while the most relevant figure is the power per unit membrane area [23]. In Ref. [22], page 347, right column, at the beginning of the "Design, construction, and operation" section, it is stated that the membrane surface is 7 cm^2, while the projected surface area is 1.6 cm^2. This leads to the evaluation of peak power density *per membrane surface* of 28 W/m^2. From Fig. S2 of supporting information of Ref. [22], curve labelled "with acid", the power density averaged over the full discharge is approximately 65% of the peak power density, thus we evaluate the power density p as 18 W/m^2. The reported energy efficiency η is 0.86% (page 347, right column, last paragraph before the "Experimental" section of Ref. [22]).

Ref. [24] reports a slightly modified setup and analysed the operation of the electrochemical cell at various temperatures. Several working temperatures are tested; here we report the results obtained for 56°C and 72°C; we put the values referring to the latter temperature in parenthesis. From Fig. 6B of Ref. [24] and from text in page 1046, right column, we see that the maximum energy efficiency is 0.5% (0.29%). According to Fig. 2A of Ref. [24] and text in page 1045, left column, the peak power density is 190 W/m^2 (236 W/m^2), but also in this case, it is normalized with respect to the "projected electrode area". In page 1047, right column, rows 2 and 8, it is stated that the membrane surface is 7 cm^2, while the projected surface area is 1.6 cm^2. This leads to the evaluation of peak power density *per membrane surface* of 43 W/m^2 (54 W/m^2). From Fig. 4 of Ref. [24], we evaluate the average power density p, 28 W/m^2 (35 W/m^2)

A different chemistry was studied in Ref. [25]. The reported peak power density is 23 W/m^2 in batch tests, normalized with respect to the "projected electrode area". In Sect. 2.2 of Ref. [25], it is stated that the cell section is 4×3 cm^2, while in page 97, left column, it is stated that the "projected electrode area" is 7 cm^2. We thus evaluate the peak power density *per membrane surface* of 13 W/m^2. From Fig. 6 of Ref. [25] we evaluate the average power density p of 8.7 W/m^2. The energy efficiency η is 0.41% (page 99, last paragraph before section 3.2.4).

Ref. [26] reports a peak power density of 45 W/m^2 (page 874, right column, last line). At the beginning of section "Results", the paper states: *"[...] the projected electrode area [...] is also the membrane area since they are the same in the AFB system)"*. From Fig. 4 of Ref. [26] we evaluate the average power density p, 22 W/m^2. The energy efficiency η is 0.7%.

Ref. [27] reports a peak power density of 119 W/m^2 (see Sect. 3.1. "Electrical power production" of Ref. [27]). It is not declared that the power is normalized

by the "projected electrode area", however, we think that this is the case, for two reasons: i) comparisons are made with the results of Refs. [22] and [22]; ii) the cell seems to be exactly equal to the cell reported by the same Authors in Ref. [25]; it must be noticed that the group of Authors of these papers is the same. In Sect. 2.1 "TRB construction and operation" of Ref. [27], it is stated that the cell section is 4×3 cm^2, while the "projected electrode area" is 7 cm^2. We thus calculate a peak power density *per membrane surface* of 69 W/m^2. From Fig. 3 of Ref. [27], we calculate the power density over the whole discharge, lasting for 220 minutes; it is approximately p=26 W/m^2. The reported energy efficiency is 0.52%.

Ref. [23] reports a theoretical work. The claimed peak power density is 45 W/m^2. Since the work is only theoretical, we do not report the performances in the literature comparison graph, Fig. 8.

In Ref. [28], two different metals (copper and zinc) are used in the two compartments of the cell. The cell always produces a voltage; during the discharge, it is 0.96 V; thanks to the thermal process, which modifies the concentration of NH_3, the charge is performed at 0.76 V. A net energy is thus gained. The energy efficiency η is 0.34%. The reported discharge peak power density is 280 W/m^2, *per membrane surface*; it must be noticed that it refers to the discharge, not to the net production of energy. From Fig. 2 of Ref. [28], we evaluate the discharge average power density as 150 W/m^2. A rough evaluation of the net power production can be done, based on the voltages: since the discharge and charge voltages are 0.96 and 0.76 V, respectively, the net energy production should be roughly (0.98-0.76)/0.98 times the discharge energy production. Moreover, we assume that the total cycle duration is twice the discharge duration. These assumptions give an average power density p=17 W/m^2.

Ref. [29] reports a system similar to Ref. [28]. The energy efficiency η is 0.45%. The reported peak power density is 26 W/m^2 *per membrane*. Repeating the calculations above, with discharge and charge voltages of 1.42 and 0.82 V, we find an average power density p=5 W/m^2. It is worth noting that the η and p are likely not evaluated in the same conditions; indeed it is stated that *"The power and energy densities can't be promoted at the same time, so the cell performance was analysed under different conditions."*.

S2.5 Thermo-osmosis (TO)

In Ref. [30], a maximum of 10.3 bar of pressure has been tested; as discussed below, much larger pressures are not feasible. The efficiency of the whole system is reported in the supplementary information of Ref. [30]. In Fig. 5b of the supplementary information of Ref. [30], the efficiency is reported as a function of the heat exchanger temperature difference ΔT_{he}. For the 10 bar curve, the value for ΔT_{he}=5 K is approximately η=0.34%. It is worth noting that this value refers to "no excess temperature difference" (see caption of the figure). According to Fig. 2g of the main paper of Ref. [30], the power density strongly decreases with decreasing excess temperature difference. We take the value of power density p of 1.5 W/m^2, corresponding to the smallest temperature difference. Likely, the

two values of η=0.34% and p=1.5 W/m^2 cannot be obtained simultaneously and they represent a large overestimation of the real (simultaneous) performances; on one hand, η=0.34% is obtained under "no excess temperature difference", and rising the temperature difference to a finite value strongly decrease η (see Fig. 6a of the supplementary information of Ref. [30]); on the other hand, decreasing the temperature difference strongly decreases p (see Fig. 2g of the main paper of Ref. [30]). However, we decided to report the overestimated values of η and p in the literature comparison graph, Fig. 8, because, although they are likely overestimated, they are however small compared to many of the other reported techniques.

Ref. [31] reports an almost completely theoretical work. The reported energy efficiency is up to 4.1%. However, this value represents an ideal thought experiment. The abstract of Ref.[31] indeed states: *"heat-to-electricity energy conversion efficiencies up to 4.1% [can be obtained]. Lower energy efficiencies, however, will occur in systems operating with high power densities ($> 5\,W/m^2$) and with finite-sized heat exchangers."* Indeed, we see that the efficiency of 4.1% is only obtained with an ideal heat recuperation, requiring infinite heat exchangers. It is thus not an experimental value. A practically relevant value can be extracted from Fig. 5 of Ref.[31]. At 80% of heat recuperation, still a practically hardly feasible value, the energy efficiency is 0.6%. Also the evaluation of power density is performed theoretically. The value of 1 W/m^2 is stated in page 12934, right column, line 6 of second paragraph of section "Implications". All the calculations reported in Ref. [31] refer to a working pressure of 50 bar, which are not feasible (see the discussion below). For this reason, we do not report data from this bibliographic reference in the literature comparison graph, Fig. 8.

Increasing the working pressure improves the performances, however, it has been shown that the pressure is limited to approximately 10 bar with the membranes that have been studied. Theoretical [32] and experimental [33] works showed that the limit of the pressure is due the membrane deformation which takes place at high pressure, which is detrimental for the vapour flux.

Thermo-osmosis can be exploited in membrane distillation desalination plants, possibly powered by low-temperature heat sources, in order to produce electrical energy together with desalinated water. Theoretical analysis [34] and experimental investigations of the physical principles [35] of the coupled processes have been carried on.

Ref. [34] is only theoretical, thus we do not report the performances in the literature comparison graph, Fig. 8. In this paper, the heat recuperation is called "ERD" and it is set to 95% heat recuperation. The paper states that the PRMD process (the membrane distillation integrated with the thermo-osmosis) can save about 0.1738 kWh/m^3 with about only 3% sacrifice of fresh water production compared to the DCMD process at the same basis. Assuming that the heat required by the whole desalination process is 7.7 kWh/m^3, with 100% heat recuperation, the efficiency of the energy production process alone would be 2.2%. The theoretically calculated power density is 2 W/m2.

Ref. [35] reports experiments and calculations on membrane distillation with

additional heat used to generate pressure (pressure-retarded thermal osmosis). The power density is 0.6 W/m^2 at 4 bar. (Fig. 2b of Ref. [35]). Since two processes are considered together, the energy efficiency of the energy production alone is not reported separately and it is difficult to estimate. From Fig. 1b of Ref. [35], at 4 bar, the energy production is 0.1 kWh/m^3 (per cubic meter of fresh water). Assuming that the heat required by the whole desalination process is 7.7 kWh/m^3, with 100% heat recuperation, the efficiency of the energy production process alone would be η=1.3%. This value however is not obtained by an experiment but it is rather a calculated value. We remark that a heat recuperation of 100% (unrealistic) is assumed. Due to the difficulty of evaluating the efficiency of the energy production process alone, and for the assumption of heat recuperation of 100%, we decided not to report the results in the literature comparison graph, Fig. 8.

Performances of highly technological carbon nanotube membranes have been discussed [36, 37]. Ref. [36] reports a theoretical model of gap-filled vertically aligned carbon nanotube membranes. The focus is on the flow. No explicit application to thermo-osmosis method is discussed. Ref. [37] is also a theoretical work, which discusses membranes based on carbon nanotubes. No performance evaluation is reported.

S2.6 Thermal separation - salinity gradient power (TS-SGP)

In this large family of techniques, the power density p is only defined by the SGP stage, while the energy efficiency η is the product of the energy efficiency of the TS and of the SGP stages, η_{TS} and η_{SGP}, respectively. The papers on the various combinations of TS and SGP techniques are now discussed. In order to evaluate η as $\eta_{TS} \cdot \eta_{SGP}$, in some cases it will be necessary to analyse more than one paper, reporting separately the evaluation of η_{TS} and η_{SGP}.

It is worth noting that, in the discussed paper on TS-SGP, the multi-effect combination is often used to reach high efficiencies. It is thoroughly discussed in Sect. S4 and 4.

S2.6.1 Vacuum distillation - pressure-retarded osmosis (VD-PRO)

Ref. [38] reports a study of a plant based on vacuum distillation coupled to pressure retarded osmosis, single and dual stage. The work report calculations based on data obtained by experiments available in literature.

Analysing Ref. [38], we find the power density in Fig. 4e, 5e and 6e: it has a maximum of 7 W/m^2.

The energy efficiency η is not explicitly reported but it can be calculated. The MED is assumed to have an electrical energy consumption P_{W-MED}. In Ref. [38], page 339, right column, line 30, the specific electrical power consumption of the MED distiller is declared to be p_{W-MED} =1.2 kWh/m^3, defined as:

$$P_{W-MED} = p_{W-MED} \cdot \dot{V} \tag{S3}$$

where $\dot{V}$ is the produced water flow.

Fig. 7b, 8b and 9b of Ref. [38] report the specific thermal consumption of the MED, S_{TC}, in the range 50-70 kWh/m^3. It is connected to the heat consumption $\dot{Q}$ by:

$$\dot{Q} = S_{TC} \cdot \dot{V} \tag{S4}$$

The power production of the PRO module is called P_{W-PRO}. The ratio P_{W-PRO}/P_{W-MED} = is reported in Fig. 7c, 8c and 9c of Ref. [38]; it reaches values up to 2. The net power production P is $P = P_{W-PRO} - P_{W-MED}$. Using the previous relations, we get:

$$\eta = \frac{P}{\dot{Q}} = \frac{p_{W-MED}}{S_{TC}} \left(P_{W-PRO}/P_{W-MED} - 1\right) \tag{S5}$$

For the two-stage system:

$$\eta = \frac{p_{W-MED}}{2 \cdot S_{TC}} \left(P_{W-PRO}/P_{W-MED} - 1\right) \tag{S6}$$

By considering the dependence of P_{W-PRO}/P_{W-MED} and S_{TC} on the various parameters, we calculate a maximum of η=0.9%. This value is also confirmed by the analysis reported in the review Ref. [2].

S2.6.2 Vacuum distillation - reverse electrodialysis (VD-RED)

The efficiency of RED devices has been discussed in the context of energy production from natural salinity differences.

Concentration H M	Efficiency η_{SGP} %	Power density p W/m^2
0.6	37.8	0.77
0.6	31.1	1.1
1.2	33.1	0.86
1.2	22.8	0.86
4.0	18.1	1.2
4.0	5.5	1.8

Table S1: Performances reported in Ref. [39].

Reference [39] reports the efficiency and power density of RED technique, at various concentrations of salt. The efficiency η_{SGP} is in the range 18–38% and the power density 0.77–1.2 W/m^2. Figure 4 of Ref. [39] shows the efficiencies and power densities for two different RED arrangements and for three different concentrations. The results are reported in Table S1. It can be noticed that the efficiency drops at increasing concentration, due to the loss of perm-selectivity. Reference [40] confirms the result above, i.e. that the efficiency of RED drops above 3.6 M. We thus see that it is not necessary to study concentrations above

4 M, even for more soluble salts, thus higher concentrations are not considered in the following. A study of mixtures of salts in RED devices has also been published [41]; the qualitative result above is confirmed also for mixtures.
Ref. [42] focuses on the vacuum distillation stage and reports the performances of single- and multiple-effect vacuum distillers.

Concentration H	single-effect η_{TS}	multiple-effect η_{TS} @ ΔT_{he}=2 K	number n of effects
M	%	%	
0.6	0.05	1.62	28
1.2	0.14	3.0	25
4.0	0.56	7.38	15

Table S2: Performances reported in Ref. [42].

The single-effect distiller efficiency η_{TS} is reported in Fig. 11a of Ref. [42]. The multiple-effect distiller efficiency η_{TS} is reported in Fig. 11a of Ref. [42]; the corresponding number n of effects is reported in Fig. 10a of Ref. [42]. The heat exchanger temperature difference is ΔT_{he}=2 K (page 681, left column) and the heat source and heat sink temperatures are T_H=100°C and T_L=25°C, respectively (page 681 of Ref. [42]). We report in Table S2 the data for three values of NaCl salt concentrations, i.e. 0.6, 1.2 and 4 M; they are obtained from the figure by interpolating the data of the nearest concentrations. It is worth noting that, for such low concentrations, the various analysed salts give approximately the same efficiency; higher concentrations are not relevant for the use of RED SGPs.
We extrapolate the efficiencies at ΔT_{he}=5 K by means of an approximate expression of the dependence of the efficiency on the ΔT_{he} (see Ref. [43, 44] and Sect. 4).

Concentration H	η_{TS} @ ΔT_{he}=5 K
M	%
0.6	0.67
1.2	1.54
4.0	4.68

Table S3: Performances extrapolated from Ref. [42] to ΔT_{he}=5 K.

We report in Table S3 the resulting η_{TS} extrapolated to ΔT_{he}=5 K.
The resulting overall efficiency η is then calculated by multiplication, $\eta = \eta_{TS} \cdot \eta_{SGP}$, with the values of Table S1. The resulting six values are reported in the literature comparison graph, Fig. 8.

The performances are in fair agreement with the values reported in Ref. [2], Fig. 6a, marked as "RED".
Ref. [1] reports the analysis and optimisation of the VD-RED process, with water solutions of NaCl and multi-effect distillation. The main results are summarised in Table 3 of Ref. [1], under the column "Reference membranes". The power density is 2.2 W/m^2 per membrane pair (p=1.1 W/m^2 per membrane area) and the energy efficiency η is 0.96%. The third column in Table 3 of Ref. [1] reports the performances envisaged with hypothetical "High-performance membranes"; no information is given on the real possibility of building such improved membranes, thus we do not consider those results. Results as a function of MEHRS performances are given in Fig. 6f of Ref. [1], but they refer to the "base case" and not to the "reference membranes", to which the above-reported data refer, so it is not possible to extrapolate the power density to the "reference membranes" scenario.
Ref. [45] extends the previous work to highly concentrated potassium acetate solutions. The obtained energy efficiency η is up to 1.6%. Also in this case, hypothetical membranes are also considered together with the real membranes. The reported performances are slightly better than the values reported above, likely thanks to the large surface of heat exchangers that is considered.
Ref. [46] reports a similar analysis, finding a maximum energy efficiency η of 1.4% and the power density is around 3 W/m^2 per membrane pair (p=1.5 W/m^2 per membrane surface).
In these last three works, reported performances are slightly better than the values reported above, likely thanks to the large surface of heat exchangers in MEHRS that is considered. They can be considered in rough agreement with the data we reported in the literature comparison graph, Fig. 8. However, it is not possible to extrapolate η or p to ΔT_{he}=5 K. For this reason, we do not report the data of this reference in the literature comparison graph, Fig. 8. However, they are discussed in Sect. S3.
Ref. [47] is a theoretical study of the performances of the VD and RED techniques. It gives an evaluation of the power density of RED devices with various solutions. Unfortunately, the membranes are assumed to be ideally permselective (Eq. 4 of Ref. [47]); this assumption leads to predict very large power densities with highly concentrated solutions (see e.g. Fig. 6A of Ref. [47], predicting 35 W/m^2 for LiBr solution). Such results are completely unrealistic. The paper also discusses the VD stage, but the assumptions are not clearly discussed. Since the work is completely theoretical, we do not report the resulting performances in the literature comparison graph, Fig. 8.
Ref. [48] reports an economical analysis of the energy production by VD-RED. The results are outside the scope of the present review.

S2.6.3 Vacuum distillation - battery mixing (VD-BattMix)

Ref. [49] reports a BattMix device working with LiCl aqueous solutions. The reported power density p is 138 mW/m^2. The efficiency of the BattMix cycle has not been evaluated.

Ref. [50] reports a device working with highly concentrated $ZnCl_2$ aqueous solutions. The reported power density p is 2 W/m^2. An improved method [51] reaches 3.7 W/m^2. In both cases, the efficiency of the BattMix cycle has not been evaluated. The efficiency of distillation η_{TS} is declared to be of the order of 10%.

S2.6.4 Vacuum distillation - redox-flow battery (VD-CRFB)

Ref. [52] reports experiments on a redox-flow battery based on NaI aqueous solutions that can be recharged by distillation. The average power density p is 10 W/m^2. The energy efficiency η_{SGP} has been evaluated experimentally, while the energy efficiency of the distiller, η_{TS}, has been evaluated based on calculations. The reported efficiency η=3% refers to a 4-effect vacuum distiller, with ΔT_{he}=6 K. Although this value is slightly more than the ΔT_{he}=5 K used as uniform basis for the comparison, we report it in the literature comparison graph, Fig. 8; the actual efficiency should be slightly higher.
Ref. [53] reports experiments on a redox-flow battery based on LiBr aqueous solutions that can be recharged by distillation. The average power density p is 6 W/m^2. The energy efficiency η_{SGP} has been evaluated experimentally, while the energy efficiency of the distiller, η_{TS}, has been evaluated based on calculations. The product is η=4%; this value refers to a single-effect vacuum distiller. No further effects can be accommodated in the considered temperature range, due to the high boiling point elevation of the solutions. No MERHS can thus come into play and the value of ΔT_{he} is not relevant. The efficiency is thus reported as it is in the literature comparison graph, Fig. 8.

S2.6.5 Membrane distillation - pressure-retarded osmosis (MD-PRO)

Ref. [54] reports a partially experimental analysis of MD-PRO. Various concentrations are studied; however, practical limitations of pressure limit the concentration to 2 M (page 5825, right column, last paragraph). We thus consider this concentration. The reported power density is 30 W/m^2 (Fig. 5 of Ref. [54]) for methanol solutions. The efficiency is reported in Fig. 6 of Ref. [54], panel b. The graphs report the efficiency as a function of the "heat recovery fraction", which refers to the heat recovery of the MEHRS. In the caption, it is stated that the process operates between T_H=318.15 K and T_L=298.15 K; we thus conclude that the "heat recovery fraction" roughly corresponding to ΔT_{he}=5 K should be 50% (see Eq. S8). From the graph (Fig. 6b of Ref. [54]) at 50% of "heat recovery" we thus find an energy efficiency of 0.8% and 1.5%, for water and methanol solutions, respectively, of LiCl.
It must be however noticed that this evaluation refers to unfeasible conditions. In page 5825 of Ref. [54], first paragraph, it is stated that the evaluation assumes that *"the energy efficiency of the PRO stage is fully maximized"*. From Fig. 6 of Ref. [54], it can be seen that, at maximum heat recovery, the efficiency approaches the Carnot efficiency. This means that the efficiency of the

PRO stage is assumed to be 100% and also the MD module is assumed to work under reversible conditions, i.e. the power production vanishes. At maximum power production, the efficiency of the PRO stage can be assumed to be 50%, and moreover the same coefficient can be applied to the MD module. We thus extrapolate p=0.2% and 0.37%, respectively, for water and methanol solutions, under finite power production.
The power density reported above can be compared with the result of Ref. [55], declaring a maximum of 18 W/m^2 for water solutions. This power density is reported in the literature comparison graph, Fig. 8, together with the efficiency found in Ref. [54] for water solutions.
Ref. [56] develops a mathematical model of the MD-PRO system. It is mainly aimed at the evaluation of the theoretical maximum efficiency of the technique. A MEHRS is applied.
[57] reports a theoretical analysis and an economical assessment. A summary of the results is given in Table 3 of Ref. [57]: the efficiency is between 0.1% and 0.8% (in agreement with our extrapolation of Ref. [54] data) and the power density of the PRO stage is between 45 and 76 W/m^2. No MEHRS is considered; this is probably the reason of the lower efficiency found in this paper compared to the previous ones. The conclusion is that the MD-PRO process is not economically viable.

S2.6.6 Membrane distillation - reverse electrodialysis (MD-RED)

Ref. [58] reports a completely theoretical work. The energy efficiency η is up to 1.2%. The power density is not declared.
In Ref. [59], the scheme of the heat recuperation is not completely described. The power density is reported in Fig. 5 of Ref. [59]; the highest value is p=2.2 W/m^2. It is however a power *per membrane pair surface* (see Eq. S23 of supporting information of Ref. [59]). Expressed *per membrane surface*, it is p=1.1 W/m^2. Exergy efficiency is shown in Fig. 6; the maximum is $\eta_{2nd-law}$=2.2%, with T_H=80°C and T_L=20°C; it corresponds to energy efficiency η=0.37%. This paper also shows that hypothetical improved membranes would give better performances.

S2.6.7 Thermolysis - pressure-retarded osmosis (TL-PRO)

Only Ref. [60] discussed this association of techniques. It is a completely theoretical work, hence we do not report the results in the literature comparison graph, Fig. 8. In Sect. 4.2 of Ref. [60], the power density is evaluated as 170 W/m^2; in the abstract, it is declared that it can exceed 200 W/m^2. In the abstract, the exergy efficiency is declared to be around 5%-10% in practical cases, with T_H=40°C and T_L=20°C; these values correspond to η=0.35%-0.7%.

S2.6.8 Thermolysis - reverse electrodialysis (TL-RED)

Ref. [61] is a theoretical analysis. The power density is p=3.5 W/m^2 and the energy efficiency is η=1.2%. The results are theoretical, and moreover are not

confirmed by subsequent papers, thus we do not report them in the literature comparison graph, Fig. 8.
Ref. [62] is a theoretical analysis based on experimental parameters. Fig. 8a reports the power density as a function of v_L. The values for v_L=0.5 and 2 cm/s are η=1.5 and 2.5 W/m^2, respectively. The power density is reported *per membrane pair* (see table of symbol definitions, page 2), thus p=0.75 and 1.25 W/m^2, respectively. Figure 10a reports the energy efficiency, η=0.2 and 0.12%, respectively, for the two values of v_L. The figures of Ref. [62] also report, in panel (b), the results for "future IEMs", which are slightly better; we do not include such hypothetical results in the literature comparison graph, Fig. 8.
Ref. [63] reports experiments on the first complete system, including both the TL and the RED stages. The performances are shown in Fig. 5 of Ref. [63]. The power density is 0.8 W/m^2 and the exergy efficiency is 0.8%, corresponding to an energy efficiency η=0.12 with T_H=80°C and T_L=25°C. The power density is reported *per membrane pair surface* (see Eq. 9 Ref. [63]), so p=0.4 W/m^2 *per membrane surface*.
Ref. [64] highlights that one of the difficulties of using ammonium bicarbonate solutions in a RED device is the formation of bubbles. The effect of flow is studied experimentally. The power density is reported in Fig. 2; the maximum power is 0.16 W/m^2. No evaluation of efficiency is performed.
Ref. [65] studies the possibility of directly coupling TL-RED with an electrolysis system, in order to produce hydrogen rather than electrical current. Various scenarios are analysed. Data from this paper are not reported in the literature comparison graph, Fig. 8.
Ref. [66] reports experiments on the RED stage. A power density of around 0.8 W/m^2 is reported under practically feasible conditions. This value confirms the result of Ref. [63]. No efficiency evaluation is performed.
Ref. [67] reports experiments on the RED stage. A power density of 0.77 W/m^2 is reported. No efficiency evaluation is performed.
Ref. [68] reports experiments on the RED stage. A power density of 0.33 W/m^2 is reported. Only the efficiency of the RED stage is evaluated.

S2.6.9 Thermolysis - microbial reverse electrodialysis RED (TL-microbial RED)

Ref. [69] reports the power densities normalised by the "cathode surface area"; they are 5.6 and 3 W/m^2 for acetate solution and domestic wastewater, respectively. The first value is not relevant in the context of this review, since acetate should be provided to the cell, while the goal here is to propose a renewable energy production by low-temperature heat sources.
The projected surface area of the cathode is 7 cm^2 (page 2, Supporting Online Material (SOP) of Ref. [69], row 9). We report instead the power density normalised by the membrane area. A single membrane is 2×4 cm^2 (page 2, Supporting Online Material (SOP) of Ref. [69], row 19); 5 chambers are stacked (page 2, Supporting Online Material (SOP) of Ref. [69], row 17). The total surface of membranes is thus 40 cm^2. The reported power density of 3 W/m^2

normalised by the "cathode surface area" thus corresponds to p=0.5 W/m^2 normalised by the membrane surface.
The energy efficiency is evaluated in terms of produced electrical work with respect to the energy input, constituted by the organic material used as a fuel for the microbial fuel cell plus the mixing free energy of the thermolytic salt solution. It is not possible to separate the two contributions. Moreover, no evaluation of the thermal separation stage is done.
In Ref. [70], the energy output is represented by production of H_2 gas, rather than by the production of electrical work. No power density is evaluated. As in the previous case, the efficiencies refer to the free energies of the incoming solutions, i.e. the fuel of the microbial fuel cell and the concentration difference of the thermolytic salt solution. Moreover, no evaluation of the thermal separation stage is done.
For these reasons, we do not report any data for these two papers in the literature comparison graph, Fig. 8.

S2.6.10 Thermolysis - Battery mixing (TL-BattMix)

Ref. [71] reports the study of electrodes for BattMix technique able to work with ammonium bicarbonate solutions. The highest power density is 6.3 mW/m^2. The efficiency of the process is not evaluated. Due to the very small power density and to the lack of an evaluation of the efficiency, we do not report the data for this paper in the literature comparison graph, Fig. 8.

S2.6.11 Other thermal separation techniques

Ref. [72] proposes to use ionic liquids which undergo a phase separation under a critical temperature (called "thermally responsive ionic liquids) in order to regenerate the concentration difference. The power production should be performed by means of PRO, with a reported power density of 2.3 W/m^2. The reported energy efficiency is very high, η=2.6% without MEHRS. This value is only calculated, based on mixing free energy and heat capacities.
The temperature *versus* entropy graph, Fig. 5 of Ref. [72], is not in scale, according to the data reported in Table 3 of Ref. [72], but the shape is likely qualitatively correct. This shape however is not consistent with the data of Table 3 of Ref. [72]. For this reason, and for the theoretical nature of the calculation of the energy efficiency, we do not discuss further this work in our review.
The idea of separating two phases by decreasing the temperature can also be pursued by means of crystallisation; it appears in a patent [73]. In this case, a BattMix approach is used to extract the mixing free energy. No evaluation of the performances of this scheme is reported in literature.

S2.7 Literature references

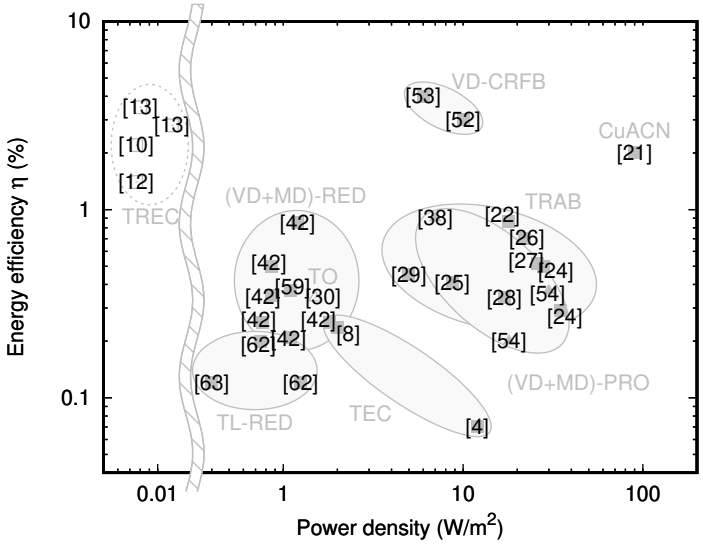

Figure S1: Literature references.

In Fig. S1 we report the numbers of the literature references used to plot the graph shown in Fig. 8. The numbers refer to the bibliography reported in this ESI and not to the bibliography numbers reported in the main paper.

S3 Detailed discussion of the literature for Sect. 4 (multi-effect combination and heat recuperation)

Here we only discuss the papers whose data are reported in the literature comparison graph, Fig. 8, according to the discussion of the previous section; exceptions are noted.

Heat exchangers between the heat source and the process and between the process and the heat sink are needed by all the discussed techniques (see Fig. 7). For this reason, they are not taken into consideration and do not participate to the heat exchanger surface S.

In the analysed papers, the heat exchangers are often characterised by ΔT_{he}, assumed as a uniform and constant temperature difference across the heat exchangers. We also make this assumption.

The discussions reported below only focus on the calculation of ρ; for discussion of η and p, see Sect. S2. Techniques in which MEHRS are not used are not

discussed here.

S3.1 Electrochemical heat engine (TREC)

MEHRS are used in the reported works on this technique. However, we decided not to report data for TREC in Fig. 11 due to the low power density (see Fig. 8) and because the reported efficiencies represent a theoretical limit value, or an overestimate, rather than the actual results of an experimental measurement.

S3.2 Membrane distillation - salinity gradient power (VD-SGP) and thermo-osmosis (TO)

In these techniques, the heat recuperation scheme (see Fig. 10), based on a counter-current heat exchanger, is used. In some paper, instead of characterising the heat exchanger with ΔT_{he}, the heat recuperation efficiency η_{rec} is used. It is defined as:

$$\eta_{rec} = \frac{\dot{Q}_{HE}}{\dot{Q}_{HE} + \dot{Q}_H} \tag{S7}$$

where $\dot{Q}_{HE}$ is the amount of heat passing through the heat exchangers (see the scheme of Fig. 10 and Ref. [74] for more detail). η_{rec} can be expressed in terms of ΔT_{he}:

$$\eta_{rec} = \frac{T_H - T_L - \Delta T_1 - \Delta T_{he}}{T_H - T_L - \Delta T_1} \tag{S8}$$

where ΔT_1 is the temperature difference between T_H and the temperature of the hot fluid entering the heat exchanger. In absence of other information, we will assume $\Delta T_1 = 0$.
In order to evaluate ρ, it is necessary to evaluate the amount of heat passing through the heat exchanger, $\dot{Q}_{HE}$. More detail of the calculation can be found in Ref. [74]. Inverting this relation:

$$\dot{Q}_{HE} = \frac{\eta_{rec}}{1 - \eta_{rec}} \dot{Q}_H \tag{S9}$$

Using the definition of η:

$$\dot{Q}_{HE} = \frac{\eta_{rec}}{1 - \eta_{rec}} \frac{1}{\eta} P \tag{S10}$$

This allows us to calculate ρ, according to Eq. 9:

$$\rho = \frac{1 - \eta_{rec}}{\eta_{rec}} \eta \cdot U \cdot \Delta T_{he} \tag{S11}$$

In turn, ΔT_{he} is calculated from η_{rec} through Eq. S8, or *vice versa*.
In the following, we use these relations for calculating ρ.

S3.2.1 Thermo-osmosis (TO)

The data reported in Fig. 11 are taken from Ref. [30]. The energy efficiency is reported in Fig. 5b of the supplementary information of Ref. [30], as a function of the heat exchanger temperature difference ΔT_{he}, for the temperature range T_L=20°C - T_H=60°C. Three curves, for three different pressures, are reported; we focus on the 10 bar. We remark again that this curve is a large overestimation, since it refers to "no excess temperature difference" and thus to vanishing power production. For this reason, it is represented as a dashed line in Fig. 11.

S3.2.2 Membrane distillation - pressure-retarded osmosis (MD-PRO)

In Ref. [54], we only consider the concentration of 2 M (page 5825, right column, last paragraph), as already explained in Sect. S2. The efficiency is reported in Fig. 6 of Ref. [54], panel b, as a function of the "heat recovery fraction" η_{rec}. In the caption, it is stated that the process operates between T_H=318.15 K and T_L=298.15 K. As explained in Sect. S2, we apply a correction factor of 0.25 to the efficiency, in order to extrapolate the efficiency to a finite power production.

S3.2.3 Membrane distillation - reverse electrodialysis (MD-RED)

Ref. [59] states: *"Regarding the MD module, the performances were enhanced accounting for heat recovery improvements and innovative module designs, which are already under development by Aquastill company."* Actually, the scheme of the heat recuperation is not completely described. It is thus not possible to evaluate ρ for this work.

S3.3 Vacuum distillation - salinity gradient power (VD-SGP)

Multi-effect combination of processes is proposed for VD-based processes. When n effects are put in series, $\dot{Q}_{HE} = (n-1)\dot{Q}_H$, because the heat exchangers are $n-1$ (excluding the first and the last shown in Fig. 7) and they are crossed approximately by the same amount of heat, $\dot{Q}_H$, since we approximate $\eta \ll 1$. We thus get:

$$\rho = \frac{P \cdot U \cdot \Delta T_{he}}{(n-1) \cdot \dot{Q}_H} \tag{S12}$$

This expression can be usefully rewritten as:

$$\rho = \frac{U \cdot \Delta T_{he} \cdot \eta}{n-1} \tag{S13}$$

In turn, n is either extracted from the analysed paper or is calculated using Eq. 15.

S3.3.1 Vacuum distillation - pressure-retarded osmosis (VD-PRO)

Ref. [38] does not report information on the temperature drop across the heat exchangers, thus it is not possible to evaluate ρ.

S3.3.2 Vacuum distillation - reverse electrodialysis (VD-RED)

The calculation follows the procedure reported in Sect. S2 for VD-RED, based on Refs. [39] and [42]. The efficiency is evaluated by multiplying η_{SGP}, Table S1, by η_{TS} for ΔT_{he}=2 K, Table S2. The value of ΔT_{he} is fixed, 2 K. The temperature range is between T_H=100°C and T_L=25°C.
The data of Ref. [42] are not reported in Fig. 11 because they refer to a single value of ΔT_{he} and thus they do not give rise to a line in the ρ *versus* η graph.
The data of Ref. [1] were not reported in Fig. 8, however they can be usefully discussed here. The effect of ΔT_{he} is shown in Fig. 6f of Ref. [1]; the horizontal axis reports the "Mean temperature difference", which can be read as the boiling point elevation (vertical line) plus the average ΔT_{he}. The graph reports the "exergy efficiency", here corresponding to $\eta_{2nd-law}$, and the "Specific HX area" in m^2/kg s. The first can be readily converted into η. The temperature range is between T_H=100°C and T_L=15°C. The number of effects is calculated as the ratio between the available temperature difference $T_H - T_L$ and the "Mean temperature difference". The values reported in Fig. 6f of Ref. [1] refer to the "base case". According to Table 3 of Ref. [1], the global exergy efficiency is increased from 2.3% to 4.3% when the "reference membranes" are taken into consideration. Thus we multiply the efficiencies of Fig. 6f of Ref. [1] by a factor 4.3/2.3.
Ref. [45] reports the data for various number of effects. The thermal efficiency is reported in Fig. 8 and the heat exchanger area per gross power is reported in Fig. 9 of Ref. [45]. We consider the lines corresponding to NaCl and KAc at 25°C, for "standard reference IEMs". The heat exchanger transfer coefficient is U=1000 W/(m^2 K) (page 6, right column of Ref. [45]). The temperature range is between T_H=100°C and T_L=15°C (page 5, right column of Ref. [45]). The parameter ρ is calculated as P/S (see Eq. 9).
Ref. [46] does not contain the information necessary to evaluate ρ.

S3.3.3 Vacuum distillation - redox-flow battery (VD-CRFB)

Ref. [52] reports an efficiency of the redox-flow battery η_{SGP}=30%. For the distillation stage, three situations are considered: two multi-effect distillers with ΔT_{he}=1 and 6 K, and a single-effect distiller (Fig. 5 of Ref. [52]). The three distillers are designed to provide 1 kW in the form of a free energy flux. The number of effects is n=5, 4, and 1. The heat inputs $\dot{Q}_H$ are 8, 10, and 40 kW, respectively, and the heat exchanger surfaces (excluding the heat exchangers from the heat source and towards the heat sink) are 64, 9.9, and 0 m^2. The heat transfer coefficient assumed in this paper is U=500 W/(m^2 K). The temperature range is T_H=100°C and T_L=25°C. The values of ρ shown in Fig. 11 are calculated from these data according to Eq. 9. The efficiencies are calculated as

$\eta = \eta_{TS} \cdot \eta_{SGP}$. The efficiency of the single-stage distiller is not represented in Fig. 11.
Ref. [53] reports an energy efficiency η=4%, with a single-effect distiller. It is not possible to fit more than one effect in the available temperature range, i.e. between T_H=100°C and T_L=25°C. The efficiency is thus represented in Fig. 11 at the top of the graph area, in a position not related to ρ, as the other techniques which do not use a MEHRS.

S3.4 Identification of literature references

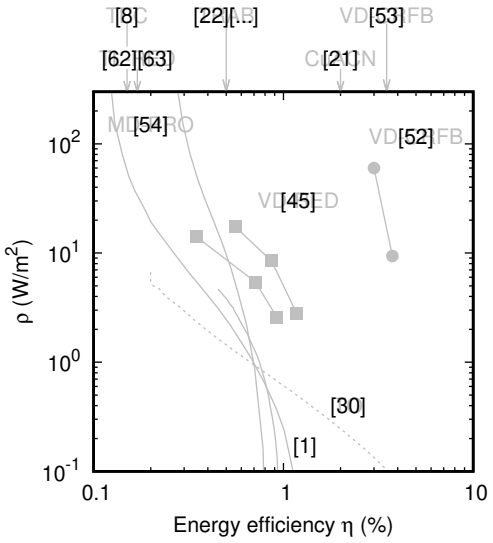

Figure S2: Literature references.

In Fig. S2 we report the numbers of the literature references used to plot the graph shown in Fig. 11. The numbers refer to the bibliography reported in this ESI and not to the bibliography numbers reported in the main paper.

S4 Comparison between ρ vs. η with theoretical curves

In this section, results reported in papers are compared to the approximate equations 16 and 17.

S4.1 Thermo-osmosis (TO)

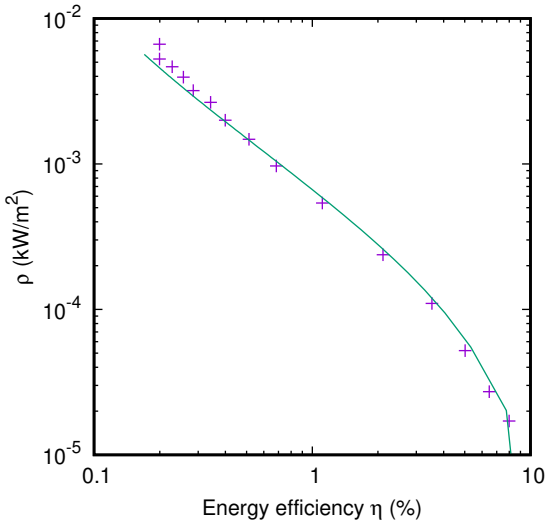

Figure S3: ρ vs. η graph for TO.

The ρ vs. η graph for TO is shown in Fig.S3. The data are extracted from Ref. [30] (see Sect. S3). Temperature range: from T_L=20°C to T_H=60°C. The curve refers to the "no excess temperature difference", thus ΔT_* corresponds to the "temperature difference" shown in Fig. 1b of Ref. [30]. The graph is not detailed enough at pressure of 10 bar and does not allow us to evaluate the temperature difference ΔT_* at 10 bar, thus we must calculate it through the procedure used to generate that graph, which is discussed in the supplementary information, Supplementary Note 1 of Ref. [30]. The result is ΔT_*=0.12 K at 10 bar of pressure difference. We assume ΔT_1=0. The value η_*=0.043% is found by fitting the curves. It is approximately the Carnot efficiency across a temperature difference ΔT_*=0.12 K, in agreement with the assumption of quasi-reversibility used to calculate the curves of Fig. 1b of Ref. [30].

S4.2 Membrane distillation - pressure-retarded osmosis (MD-PRO)

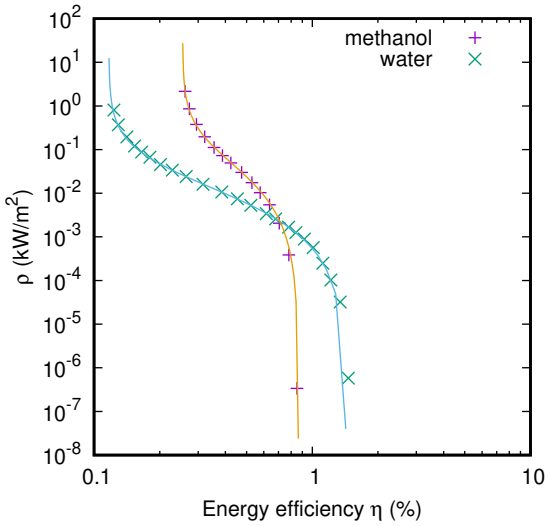

Figure S4: ρ vs. η graph for MD-PRO.

The ρ vs. η graph for MD-PRO is shown in Fig.S4. The data are extracted from Ref. [54] (see Sect. S3). The efficiency is reported in Fig. 6 of Ref. [54], panel b, as a function of the "heat recovery fraction" η_{rec} (see Sect. S3 for the choice of 2 M solutions). The temperature range is between T_L=298.15 K and T_H=318.15 K. The values of ΔT_* and η_* are obtained by fitting. We get ΔT_*=15 and 3.2 K for methanol and water solutions, respectively, and η_*=0.36% and 0.13%, respectively. The values of ΔT_* are much larger than the boiling point elevations of the 2 M solutions, 3.44 and 2 K for methanol and water solutions, respectively (obtained from the ebullioscopic constant of the solvents). Indeed, in membrane distillation such values represent the "threshold temperature difference", while the actual temperature difference across the membrane is usually much larger.

S4.3 Vacuum distillation - reverse electrodialysis (VD-RED)

Ref. [42] discusses the VD-RED technique, but mainly focuses on the efficiency of the distillation process.

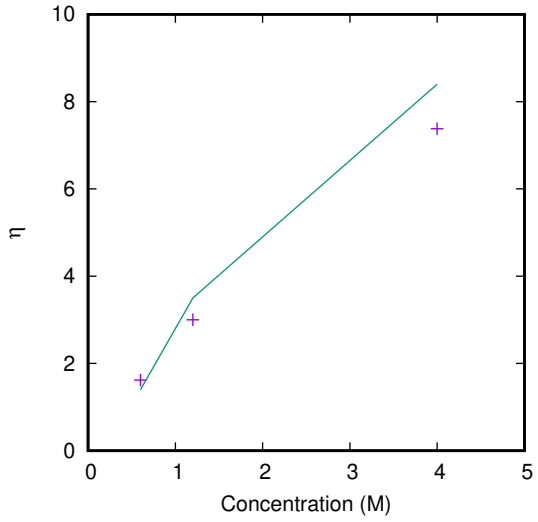

Table S4: ρ vs. η graph for VD-RED.

We already reported data from Ref. [42] in Table S2. The table reports the single-effect efficiency η_{TS}, the multiple-effect efficiency η_{TS} and the number n of effects. Fig. S4 reports the comparison with Eq. 16, using the single-effect efficiency as η_*.

Concentration H	ΔT_*	η_*
M	K	%
0.6	0.5508	0.0189
0.6	0.5508	0.01555
1.2	1.1016	0.04634
1.2	1.1016	0.03192
4.0	3.672	0.10136
4.0	3.672	0.0308

Table S5: Parameters of the VD-RED technique calculated from Ref. [42] for NaCl solutions

The overall η_* is then calculated using η_{SGP} of Table S1. The value of ΔT_* is calculated as the boiling point elevation of the salt solution. The results are shown in Table S5.
Refs. [1] and [45] do not report enough detail to perform the comparison of their results with Eqs. 16 and 17.

S4.4 Vacuum distillation - redox-flow battery (VD-CRFB)

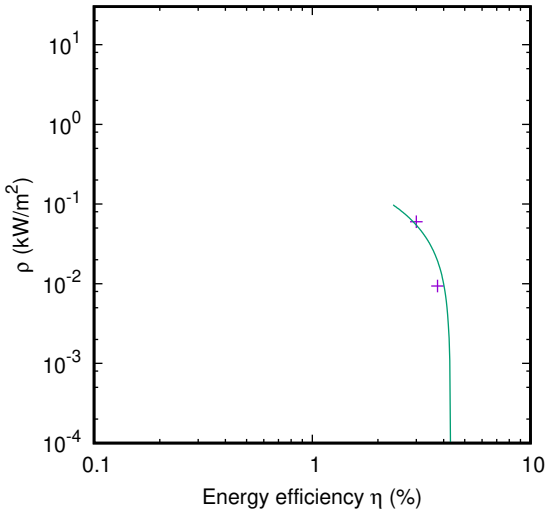

Figure S5: ρ vs. η graph for VD-CRFB.

The ρ vs. η graph for VD-CRFB is shown in Fig.S5. The data are extracted from Ref. [52] (see Sect. S3). In Ref. [52], the value of ΔT_* is given explicitly: it corresponds to the boiling point elevation of the used solution, ΔT_*=17 K. The single-effect distiller efficiency η_{TS} is 2.5%; multiplying by η_{SGP}=30%, we get η_*=0.75%. The value used to fit the data in the graph is 30% larger. The line in the graph represents the theoretical evaluation based on Eqs. 16 and 17.

S4.5 Identification of the literature references

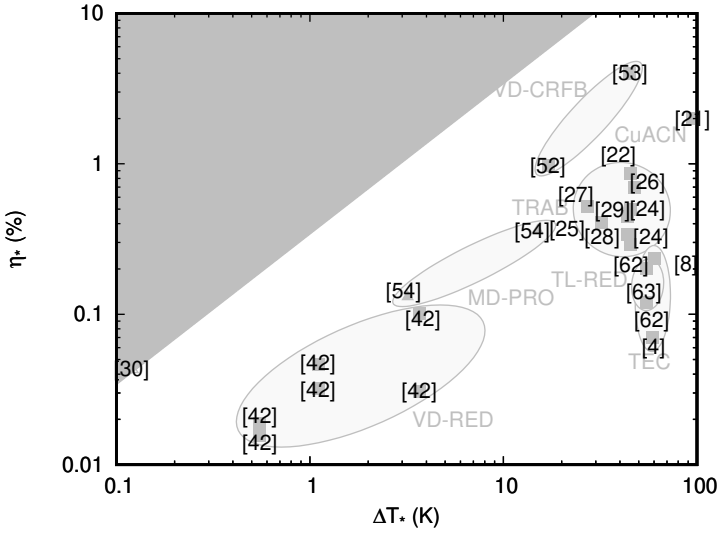

Figure S6: Position of the literature references on the η_* *versus* ΔT_* graph.

In Fig. S6 we report the numbers of the literature references used to plot the graph shown in Fig. 12. The numbers refer to the bibliography reported in this ESI and not to the bibliography numbers reported in the main paper.

S5 Considerations on industrial waste heat

It must be noticed that, in several industrial processes, methods for recycling the waste heat into the process itself are already available and are often installed. There is a trade-off between the complexity and the capital cost of the required equipment and (the increase of) the temperature of the released heat. Indeed, using larger heat exchangers enables the exploitation of the heat down to a lower temperature, however, heat exchangers represent an economic cost, occupy a significant volume and contribute to the complexity of the system.
Heat below 100°C is often released simply because the savings from exploiting it further (to lower temperature) do not pay back the needed increase of complexity, size, and capital cost of the needed heat exchangers.
Heat exchangers are needed for all the techniques discussed here (see Sect. 3). In some of them, they represent a significant cost, as noticed in Ref. [1]: *" the amount of heat exchanger area [...] [represents] an important share of the total capital costs of the unit. "*. All the techniques introduce additional complexity and cost to the system. It is thus questionable if the application of such

techniques can provide a better exploitation of this fraction of waste heat, or it could be more conveniently recovered simply by extending the application of the already existing processes. For these reasons, the large-scale application to industrial waste heat recovery is considered in this review as marginally relevant.

S6 Cost of solar heat collection

Here we consider the collection of solar heat with a household-scale system, based on state-of-the-art stationary non-imaging optics [75] coupled with vacuum tubes and selective adsorbers [76], similar to the ones normally used for domestic hot water production.
The cost of such collectors is of the order of 130 €/m^2 (see e.g. Ref. [77]). As a comparison, the cost of a complete installed photovoitaic system is around 300-400 €/m^2, a minor fraction of which is the cost of the solar cells. We can assume that the cost of the solar heat collectors and their installation is 200 €/m^2.
Working at 100°C, with a concentration factor of 2 and CERMET-based selective absorbers [78], 95% of sun power is collected. A peak power of 950 W/m^2 under standard conditions can be obtained. We thus evaluate a cost per installed unit heat power of 0.2 €/W.

S7 Cost per unit surface area

Here we report the typical cost per unit surface area of the various techniques. The most common elements seen in the discussed techniques are perm-selective ion-exchange membranes. They are needed by CuACN, TRAB and RED-based TS-SGP techniques. Moreover, some TECs and TRECs also require such membranes.
Nafion membranes are used in several industrial applications. They are sold at prices around 300-700 €/m^2; in a work on PEM cells [79], the cost is assumed to be 550 €/m^2. The cost of the membranes is high for RED applications and hinders the development of RED for exploiting naturally occurring salinity gradients. Ongoing research is focusing on reducing the price of membranes for this application. For example, Fujifilm developed a specific line for the so-called "blue energy", however, the market price is still high, around 80 €/m^2 *per membrane*, and two membranes per cell are used in RED.
The PRO technique, used in the TS-SGP association, requires semipermeable membranes. Such membranes are industrially used in reverse osmosis for water desalination. A recent work on reverse osmosis and PRO [80] evaluates the cost of PRO membranes in a range between 30 and 60 \$/m^2.
Some of the TECs and TRECs make use of electrodes that are similar to the ones used in batteries. As a reference, we consider the cost of electrodes used in lithium-ion batteries. The cost of such electrodes per unit surface can be evaluated assuming mass loading of active material of 20 mg/cm^2 [81], charge density of the active material 180 mAh/g, and typical cost of lithium-ion bat-

teries of 600 €/kWh, giving a rough evaluation of 77 €/m^2. It is worth noting that a significant part of the cost comes from manufacturing, so it cannot be decreased too much by selecting cheaper materials; this price can give a rough idea of the costs of TECs and TRECs not using membranes.
The ceramic membranes used in CRFBs are currently not used industrially. The precursors are cheap, e.g. 2 €/m^2 for a 100 μm-thick layer of NASICON. However, the manufacturing cost is not reported in papers on CRFB and it is difficult to make an evaluation of the cost of a real production.
TO is based on hydrophobic porous membranes, which are industrially used in membrane distillation. The cost is typically assumed to be around 100 €/m^2, see Ref. [82].

References

[1] B. Ortega-Delgado, F. Giacalone, P. Catrini, A. Cipollina, A. Piacentino, A. Tamburini, G. Micale, Reverse electrodialysis heat engine with multi-effect distillation: Exergy analysis and perspectives, Energy Conversion and Management 194 (2019) 140–159. doi:10.1016/j.enconman.2019.04.056.

[2] M. Rahimi, A. P. Straub, F. Zhang, X. Zhu, M. Elimelech, C. A. Gorski, B. E. Logan, Emerging electrochemical and membrane-based systems to convert low-grade heat to electricity, Energy & Environmental Science 11 (2) (2018) 276–285. doi:10.1039/c7ee03026f.

[3] M. F. Dupont, D. R. MacFarlane, J. M. Pringle, Thermo-electrochemical cells for waste heat harvesting – progress and perspectives, Chem. Commun. 53 (2017) 6288–6302. doi:10.1039/C7CC02160G.

[4] L. Zhang, T. Kim, N. Li, T. J. Kang, J. Chen, J. M. Pringle, M. Zhang, A. H. Kazim, S. Fang, C. Haines, D. Al-Masri, B. A. Cola, J. M. Razal, J. Di, S. Beirne, D. R. MacFarlane, A. Gonzalez-Martin, S. Mathew, Y. H. Kim, G. Wallace, R. H. Baughman, High power density electrochemical thermocells for inexpensively harvesting low-grade thermal energy, Adv. Mater. 29 (1605652). doi:10.1002/adma.201605652.

[5] H. Im, T. Kim, H. Song, J. Choi, J. S. Park, R. Ovalle-Robles, H. D. Yang, K. D. Kihm, R. H. Baughman, H. H. Lee, T. J. Kang, Y. H. Kim, High-efficiency electrochemical thermal energy harvester using carbon nanotube aerogel sheet electrodes, Nat. Commun. 7 (10600) (2016) 1–7. doi:10.1038/ncomms10600.

[6] J. Duan, G. Feng, B. Yu, J. Li, M. Chen, P. Yang, J. Feng, K. Liu, J. Zhou, Aqueous thermogalvanic cells with a high Seebeck coefficient for low-grade heat harvest, Nature Comm. 9 (5146) (2018) 1–8. doi:10.1038/s41467-018-07625-9.

[7] W. M. Haynes, CRC Handbook of Chemistry and Physics, CRC press, 2015.

[8] R. Hu, B. A. Cola, N. Haram, J. N. Barisci, S. Lee, S. Stoughton, G. Wallace, C. Too, M. Thomas, A. Gestos, M. E. d. Cruz, J. P. Ferraris, A. A. Zakhidov, R. H. Baughman, Harvesting waste thermal energy using a carbon-nanotube-based thermo-electrochemical cell, Nano Lett. 10 (3) (2010) 838–846. doi:10.1021/nl903267n.

[9] A. Lazar, D. Al-Masri, D. R. MacFarlane, J. M. Pringle, Enhanced thermal energy harvesting performance of a cobalt redox couple in ionic liquidsolvent mixtures, Phys. Chem. Chem. Phys. 18 (3) (2016) 1404. doi:10.1039/C5CP04305K.

[10] S. W. Lee, Y. Yang, H.-W. Lee, H. Ghasemi, D. Kraemer, G. Chen, Y. Cui, An electrochemical system for efficiently harvesting low-grade heat energy, Nature Communications 5 (2014) 3942. doi:10.1038/ncomms4942.

[11] D. Brogioli, et al., Exploiting the spontaneous potential of the electrodes used in capacitive mixing technique for extraction of salinity-difference energy, Energ. Environ. Sci. 5 (12) (2012) 9870–9880.

[12] Y. Yang, S. W. Lee, H. Ghasemi, J. Loomis, X. Li, D. Kraemer, G. Zheng, Y. Cui, G. Chen, Charging-free electrochemical system for harvesting low-grade thermal energy, Proc. Natl. Acad. Sci. U. S. A. 111 (2014) 17011. doi:10.1073/pnas.1415097111.

[13] Y. Yang, J. Loomis, H. Ghasemi, S. W. Lee, Y. J. Wang, Y. Cui, G. Chen, Membrane-free battery for harvesting low-grade thermal energy, Nano Lett. 14 (2014) 6578. doi:10.1021/nl5032106.

[14] R. H. Hammond, W. M. Risen, An electrochemical heat engine for direct solar energy conversion, Solar Energy 23 (1979) 443–449. doi:10.1016/0038-092X(79)90153-1.

[15] X. Wang, Y.-T. Huang, C. Liu, K. Mu, K. H. Li, S. Wang, C.-H. Su, S.-P. Feng, Direct thermal charging cell for converting low-grade heat to electricity, Nature Communications 10 (2019) 4151–4158. doi:10.1038/s41467-019-12144-2.

[16] A. D. Poletayev, I. S. McKay, W. C. Chueh, A. Majumdar, Continuous electrochemical heat engines, Energy Environ. Sci. 11 (2018) 2964–2971. doi:10.1039/c8ee01137k.

[17] S. Ahualli, M. M. Fernandez, G. Iglesias, A. V. Delgado, L. L. Jimenez, Temperature effects on energy production by salinity exchange, Environ. Sci. Tech. 48 (20) (2014) 12378–12385. doi:10.1021/es500634f.

[18] B. B. Sales, O. S. Burheim, S. Porada, V. Presser, C. J. N. Buisman, H. V. M. Hamelers, Extraction of energy from small thermal differences near room temperature using capacitive membrane technology, Environ. Sci. Technol. Lett. 1 (9) (2014) 356–360. doi:10.1021/ez5002402.

[19] A. Härtel, M. Janssen, D. Weingarth, V. Presser, R. van Roij, Heat-to-current conversion of low-grade heat from a thermocapacitive cycle by supercapacitors, Energy Environ. Sci. 8 (8) (2015) 2396–2401. doi:10.1039/c5ee01192b.

[20] P. Peljo, D. Lloyd, D. Nguyet, M. Majaneva, K. Kontturi, Towards a thermally regenerative all-copper redox flow battery, Phys. Chem. Chem. Phys. 16 (2014) 2831–2835. doi:10.1039/c3cp54585g.

[21] S. Maye, H. H. Girault, P. Peljo, Thermally regenerative copper nanoslurry flow batteries for heat-to-power conversion with low-grade thermal energy, Energy & Environmental Sciencedoi:10.1039/D0EE01590C.

[22] F. Zhang, J. Liu, W. Yang, B. E. Logan, A thermally regenerative ammonia-based battery for efficient harvesting of low-grade thermal energy as electrical power, Energ. Environ. Sci. 8 (2015) 343–349. doi:10.1039/C4EE02824D.

[23] H. Tian, W. Jiang, G. Q. Shu, W. G. Wang, D. X. Huo, M. Z. Shakir, Analysis and optimization of thermally-regenerative ammonia-based flow battery based on a 3-d model, J. Electrochem. Soc. 166 (13) (2019) A2814–A2825. doi:10.1149/2.0711912jes.

[24] F. Zhang, N. La Barge, W. Yang, J. Liu, B. E. Logan, Enhancing low-grade thermal energy recovery in a thermally regenerative ammonia battery using elevated temperatures, ChemSusChem 8 (6) (2015) 1043–1048. doi:10.1002/cssc.201403290.

[25] M. Rahimi, T. Kim, C. A. Gorski, B. E. Logan, A thermally regenerative ammonia battery with carbon-silver electrodes for converting low-grade waste heat to electricity, Journal of Power Sources 373 (2018) 95–102. doi:10.1016/j.jpowsour.2017.10.089.

[26] X. Zhu, M. Rahimi, C. A. Gorski, B. Logan, A thermally-regenerative ammonia-based flow battery for electrical energy recovery from waste heat, ChemSusChem 9 (8) (2016) 873–9. doi:10.1002/cssc.201501513.

[27] M. Rahimi, A. D'Angelo, C. A. Gorski, O. Scialdone, B. E. Logan, Electrical power production from low–grade waste heat using a thermally regenerative ethylenediamine battery, J. Power Sources 351 (2017) 45–50. doi:10.1016/j.jpowsour.2017.03.074.

[28] W. G. Wang, G. Q. Shu, H. Tian, D. X. Huo, X. P. Zhu, A bimetallic thermally-regenerative ammonia-based flow battery for low-grade waste

heat recovery, J. Power Sources 424 (2019) 184–192. doi:10.1016/j.jpowsour.2019.03.086.

[29] W. G. Wang, H. Tian, G. Q. Shu, D. X. Huo, F. Zhang, X. P. Zhu, A bimetallic thermally regenerative ammonia-based battery for high power density and efficiently harvesting low-grade thermal energy, J. Mat. Chem. A 7 (11) (2019) 5991–6000. doi:10.1039/c8ta10257k.

[30] A. P. Straub, N. Y. Yip, S. H. Lin, J. Lee, M. Elimelech, Harvesting low-grade heat energy using thermo-osmotic vapour transport through nanoporous membranes, Nature Energy 1 (2016) 16090. doi:10.1038/NENERGY.2016.90.

[31] A. P. Straub, M. Elimelech, Energy efficiency and performance limiting effects in thermo-osmotic energy conversion from low-grade heat, Environ. Sci. Technol. 51 (21) (2017) 12925–12937. doi:10.1021/acs.est.7b02213.

[32] X. Chen, C. Boo, N. Y. Yip, Low-temperature heat utilization with vapor pressure-driven osmosis: Impact of membrane properties on mass and heat transfer, J. Membr. Sci. 588 (2019) 117181. doi:10.1016/j.memsci.2019.117181.

[33] Z. W. Yuan, L. Wei, J. D. Afroze, K. Goh, Y. M. Chen, Y. X. Yu, Q. H. She, Y. Chen, Pressure-retarded membrane distillation for low-grade heat recovery: The critical roles of pressure-induced membrane deformation, J. Membr. Sci. 579 (2019) 90–101. doi:10.1016/j.memsci.2019.02.045.

[34] K. Park, D. Y. Kim, D. R. Yang, Theoretical analysis of pressure retarded membrane distillation (PRMD) process for simultaneous production of water and electricity, Industrial & Engineering Chemistry Research 56 (50) (2017) 14888–14901. doi:10.1021/acs.iecr.7b03642.

[35] Z. W. Yuan, Y. X. Yu, L. Wei, X. Sui, Q. H. She, Y. Chen, Pressure-retarded membrane distillation for simultaneous hypersaline brine desalination and low-grade heat harvesting, J. Membr. Sci. 597 (2020) 117765. doi:10.1016/j.memsci.2019.117765.

[36] X. K. Liu, L. S. Shu, S. P. Jin, A modeling investigation on the thermal effect in osmosis with gap-filled vertically aligned carbon nanotube membranes, J. Membr. Sci. 580 (2019) 143–153. doi:10.1016/j.memsci.2019.03.002.

[37] L. Fu, S. Merabia, L. Joly, Understanding fast and robust thermo-osmotic flows through carbon nanotube membranes: Thermodynamics meets hydrodynamics, J. Phys. Chem. Letters 9 (8) (2018) 2086–2092. doi:10.1021/acs.jpclett.8b00703.

[38] A. Altaee, P. Palenzuela, G. Zaragoza, A. A. AlAnezi, Single and dual stage closed-loop pressure retarded osmosis for power generation: Feasibility and performance, Applied Energy 191 (2017) 328–345. doi:10.1016/j.apenergy.2017.01.073.

[39] N. Y. Yip, M. Elimelech, Comparison of energy efficiency and power density in pressure retarded osmosis and reverse electrodialysis, Environ. Sci. Technol. 48 (18) (2014) 11002–11012. doi:10.1021/es5029316.

[40] X. Zhu, W. He, B. E. Logan, Influence of solution concentration and salt types on the performance of reverse electrodialysis cells, Journal of Membrane Science 494 (2015) 154–160. doi:10.1016/j.memsci.2015.07.053.

[41] M. Micari, M. Bevacqua, A. Cipollina, A. Tamburini, W. Van Baak, T. Putts, G. Micale, Effect of different aqueous solutions of pure salts and salt mixtures in reverse electrodialysis systems for closed-loop applications, J. Membr. Sci. 551 (2018) 315–325. doi:10.1016/j.memsci.2018.01.036.

[42] F. Giacalone, C. Olkis, G. Santori, A. Cipollina, S. Brandani, G. Micale, Novel solutions for closed-loop reverse electrodialysis: Thermodynamic characterisation and perspective analysis, Energy 166 (2019) 674–689. doi:10.1016/j.energy.2018.10.049.

[43] D. Brogioli, F. La Mantia, N. Y. Yip, Thermodynamic analysis and energy efficiency of thermal desalination processes, Desalination 428 (2018) 29–39. doi:10.1016/j.desal.2017.11.010.

[44] D. Brogioli, F. La Mantia, N. Y. Yip, Energy efficiency analysis of distillation for thermally regenerative salinity gradient power technologies, Renewable Energy 133 (2019) 1034–1045. doi:10.1016/j.renene.2018.10.107.

[45] B. Ortega-Delgado, F. Giacalone, A. Cipollina, M. Papapetrou, G. Kosmadakis, A. Tamburini, G. Micale, Boosting the performance of a reverse electrodialysis - multi-effect distillation heat engine by novel solutions and operating conditions, Appl. Energy 253 (2019) 113489. doi:10.1016/j.apenergy.2019.113489.

[46] P. Palenzuela, M. Micari, B. Ortega-Delgado, F. Giacalone, G. Zaragoza, D. C. Alarcon-Padilla, A. Cipollina, A. Tamburini, G. Micale, Performance analysis of a RED-MED salinity gradient heat engine, Energies 11 (12) (2018) 3385. doi:10.3390/en11123385.

[47] A. Tamburini, M. Tedesco, A. Cipollina, G. Micale, M. Ciofalo, M. Papapetrou, W. Van Baak, A. Piacentino, Reverse electrodialysis heat engine for sustainable power production, Applied Energy 206 (2017) 1334–1353. doi:10.1016/j.apenergy.2017.10.008.

[48] M. Papapetrou, G. Kosmadakis, F. Giacalone, B. Ortega-Delgado, A. Cipollina, A. Tamburini, G. Micale, Evaluation of the economic and environmental performance of low-temperature heat to power conversion using a reverse electrodialysis - multi-effect distillation system, Energies 12 (17). doi:10.3390/en12173206.

[49] F. La Mantia, M. Pasta, H. D. Deshazer, B. E. Logan, Y. Cui, Batteries for efficient energy extraction from a water salinity difference, Nano Lett. 11 (2011) 1810–1813. doi:10.1021/nl200500s.

[50] M. Marino, L. Misuri, A. Carati, D. Brogioli, Proof-of-concept of a zinc-silver battery for the extraction of energy from a concentration difference, Energies 7 (6) (2014) 3664–3683. doi:10.3390/en7063664.

[51] M. Marino, L. Misuri, A. Carati, D. Brogioli, Boosting the voltage of a salinity-gradient-power electrochemical cell by means of complex-forming solutions, Appl. Phys. Lett. 105 (2014) 033901. doi:10.1063/1.4890976.

[52] I. Facchinetti, R. Ruffo, F. La Mantia, D. Brogioli, Thermally-regenerable redox flow battery for exploiting low-temperature heat sources, Cell Reports Physical Science 1 (5) (2020) 100056. doi:10.1016/j.xcrp.2020.100056.

[53] I. Facchinetti, E. Cobani, D. Brogioli, F. La Mantia, R. Ruffo, Thermally regenerable redox flow battery, ChemSusChem 13 (2020) 5460–5467. doi:10.1002/cssc.202001799.

[54] E. Shaulsky, C. Boo, S. H. Lin, M. Elimelech, Membrane-based osmotic heat engine with organic solvent for enhanced power generation from low-grade heat, Environ. Sci. Tech. 49 (9) (2015) 5820–5827. doi:10.1021/es506347j.

[55] D. Anastasio, J. T. Arena, E. A. Cole, J. R. McCutcheon, Impact of temperature on power density in closed-loop pressure retarded osmosis for grid storage, Journal of Membrane Science 479 (2015) 240–245. doi:10.1016/j.memsci.2014.12.046.

[56] S. H. Lin, N. Y. Yip, T. Y. Cath, C. O. Osuji, M. Elimelech, Hybrid pressure retarded osmosis-membrane distillation system for power generation from low-grade heat: thermodynamic analysis and energy efficiency, Environ. Sci. Techn. 48 (9) (2014) 5306–5313. doi:10.1021/es405173b.

[57] K. L. Hickenbottom, J. Vanneste, L. Miller-Robbie, A. Deshmukh, M. Elimelech, M. B. Heeley, T. Y. Cath, Techno-economic assessment of a closed-loop osmotic heat engine, Journal of Membrane Science 535 (2017) 178–187. doi:10.1016/j.memsci.2017.04.034.

[58] R. Long, B. Li, Z. Liu, W. Liu, Hybrid membrane distillation-reverse electrodialysis electricity generation system to harvest low-grade thermal energy, J. Memb. Sci. 525 (2017) 107–115. doi:10.1016/j.memsci.2016.10.035.

[59] M. Micari, A. Cipollina, F. Giacalone, G. Kosmadakis, M. Papapetrou, G. Zaragoza, G. Micale, A. Tamburini, Towards the first proof of the concept of a reverse electrodialysis - membrane distillation heat engine, Desalination 453 (2019) 77–88. doi:10.1016/j.desal.2018.11.022.

[60] R. L. McGinnis, J. R. McCutcheon, M. Elimelech, A novel ammonia-carbon dioxide osmotic heat engine for power generation, J. Membr. Sci. 305 (1–2) (2007) 13–19. doi:10.1016/j.memsci.2007.08.027.

[61] M. Bevacqua, A. Tamburini, M. Papapetrou, A. Cipollina, G. Micale, A. Piacentino, Reverse electrodialysis with NH_4HCO_3-water systems for heat-to-power conversion, Energy 137 (2017) 1293–1307. doi:10.1016/J.ENERGY.2017.07.012.

[62] F. Giacalone, F. Vassallo, L. Griffin, M. C. Ferrari, G. Micale, F. Scargiali, A. Tamburini, A. Cipollina, Thermolytic reverse electrodialysis heat engine: model development, integration and performance analysis, Energy Conversion and Management 189 (2019) 1–13. doi:10.1016/j.enconman.2019.03.045.

[63] F. Giacalone, F. Vassallo, F. Scargiali, A. Tamburini, A. Cipollina, G. Micale, The first operating thermolytic reverse electrodialysis heat engine, J. Membr. Sci. 595 (2020) 117522. doi:10.1016/j.memsci.2019.117522.

[64] M. C. Hatzell, B. E. Logan, Evaluation of flow fields on bubble removal and system performance in an ammonium bicarbonate reverse electrodialysis stack, J. Membr. Sci. 446 (2013) 449–455. doi:10.1016/j.memsci.2013.06.019.

[65] M. C. Hatzell, I. Ivanov, R. D. Cusick, X. P. Zhu, B. E. Logan, Comparison of hydrogen production and electrical power generation for energy capture in closed-loop ammonium bicarbonate reverse electrodialysis systems, Phys. Chem. Chem. Phys. 16 (4) (2014) 1632–1638. doi:10.1039/c3cp54351j.

[66] D. H. Kim, B. H. Park, K. Kwon, L. Li, D. Kim, Modeling of power generation with thermolytic reverse electrodialysis for low-grade waste heat recovery, Applied Energy 189 (2017) 201–210. doi:10.1016/j.apenergy.2016.10.060.

[67] K. Kwon, B. H. Park, D. H. Kim, D. Kim, Parametric study of reverse electrodialysis using ammonium bicarbonate solution for low-grade waste heat recovery, Energy Conversion and Management 103 (2015) 104–110. doi:10.1016/j.enconman.2015.06.051.

[68] X. Luo, X. Cao, Y. Mo, K. Xiao, X. Zhang, P. Liang, X. Huang, Power generation by coupling reverse electrodialysis and ammonium bicarbonate: Implication for recovery of waste heat, Electrochem. Comm. 19 (2012) 25–28. doi:10.1016/j.elecom.2012.03.004.

[69] R. D. Cusick, Y. Kim, B. E. Logan, Energy capture from thermolytic solutions in microbial reverse-electrodialysis cells, Science 335 (6075) (2012) 1474–1477. doi:10.1126/science.1219330.

[70] J. Y. Nam, R. D. Cusick, Y. Kim, B. E. Logan, Hydrogen generation in microbial reverse-electrodialysis electrolysis cells using a heat-regenerated salt solution, Environ. Sci. Techn. 46 (2012) 5240–5246. doi:10.1021/es300228m.

[71] T. Kim, M. Rahimi, B. E. Logan, C. Gorski, Evaluating battery-like reactions to harvest energy from salinity differences using ammonium bicarbonate salt solutions, ChemSusChem 9 (9) (2016) 981–988. doi:10.1002/cssc.201501669.

[72] Y. Zhong, X. Wang, X. Feng, S. Telalovic, Y. Gnanou, K.-W. Huang, X. Hu, Z. Lai, Osmotic heat engine using thermally responsive ionic liquids, Environ. Sci. Technol. 51 (16) (2017) 9403–9409. doi:10.1021/acs.est.7b02558.

[73] V. Styliaras, Electric energy production by voltaic cell solution temperature change, patent WO 2008059297 A1, 2008 (2008).

[74] D. Brogioli, F. L. Mantia, Heat recovery in energy production from low temperature heat sources, AIChE Journal 65 (2019) 980–991. doi:10.1002/aic.16496.

[75] Y. Tian, C. Y. Zhao, A review of solar collectors and thermal energy storage in solar thermal applications, Applied Energy 104 (2013) 538–553. doi:10.1016/j.apenergy.2012.11.051.

[76] P. Bermel, K. Yazawa, J. L. Gray, X. Xu, A. Shakouri, Hybrid strategies and technologies for full spectrum solar conversion, Energy & Environmental Science 9 (9) (2016) 2776–2788. doi:10.1039/c6ee01386d.

[77] S. Kalogirou, Thermal performance, economic and environmental life cycle analysis of thermosiphon solar water heaters, Solar Energy 83 (1) (2009) 39–48. doi:10.1016/j.solener.2008.06.005.

[78] F. Cao, K. McEnaney, G. Chen, Z. F. Ren, A review of cermet-based spectrally selective solar absorbers, Energy & Environmental Science 7 (5) (2014) 1615–1627. doi:10.1039/c3ee43825b.

[79] S. K. Kamarudin, W. R. W. Daud, A. M. Som, M. Takriff, A. W. Mohammad, Technical design and economic evaluation of a PEM fuel cell system, J. Power Sources (2006) 641–649.

[80] N. Sawaki, C.-L. Chen, Cost evaluation for a two-staged reverse osmosis and pressure retarded osmosis desalination process, Desalination 497 (2021) 114767. doi:10.1016/j.desal.2020.114767.

[81] G. Lenze, H. Bockholt, C. Schilcher, L. Froböse, D. Jansen, U. Krewer, A. Kwade, Impacts of variations in manufacturing parameters on performance of lithium-ion-batteries, J. Electrochem. Society 165 (2) (2018) A314–A322.

[82] M. Khayet, Solar desalination by membrane distillation: Dispersion in energy consumption analysis and water production costs (a review), Desalination 308 (2013) 89–101. doi:10.1016/j.desal.2012.07.010.